Cosmological constraints on very dark photons

Anthony Fradette,[1] Maxim Pospelov,[1,2] Josef Pradler,[3] and Adam Ritz[1]
[1]Department of Physics and Astronomy, University of Victoria, Victoria, British Columbia V8P 5C2, Canada
[2]Perimeter Institute for Theoretical Physics, Waterloo, Ontario N2J 2W9, Canada
[3]Institute of High Energy Physics, Austrian Academy of Sciences, A-1050 Vienna, Austria
(Received 10 July 2014; published 25 August 2014)

We explore the cosmological consequences of kinetically mixed dark photons with a mass between 1 MeV and 10 GeV and an effective electromagnetic fine structure constant as small as 10^{-38}. We calculate the freeze-in abundance of these dark photons in the early universe and explore the impact of late decays on big bang nucleosynthesis and the cosmic microwave background. This leads to new constraints on the parameter space of mass m_V vs kinetic mixing parameter κ.

DOI: 10.1103/PhysRevD.90.035022 PACS numbers: 12.60.Cn, 12.60.-i, 14.80.-j, 95.35.+d

I. INTRODUCTION

In the past two decades, there has been impressive progress in our understanding of the cosmological history of the Universe. A variety of precision measurements and observations point to a specific sequence of major cosmological events: inflation, baryogenesis, big bang nucleosynthesis (BBN), recombination and the decoupling of the cosmic microwave background (CMB). While our knowledge of inflation and baryogenesis, likely linked to the earliest moments in the Universe, is necessarily more uncertain, BBN and the CMB have a firm position in cosmic chronology. This by itself puts many models of particle physics to a stringent test, as the increasing precision of cosmological data leaves less and less room for deviations from the minimal scenario of standard cosmology. In this paper, we adhere to the standard cosmological model, taking as given the above sequence of the main cosmological events. Thus we assume that the Universe emerged from the last stage of inflation and baryogenesis well before the onset of BBN. These minimal assumptions will allow us to set stringent bounds on very weakly interacting sectors of new physics beyond the Standard Model (SM).

Neutral hidden sectors, weakly coupled to the Standard Model, are an intriguing possibility for new physics. They are motivated on various fronts, e.g. in the form of right-handed neutrinos allowing for neutrino oscillations, or by the need for nonbaryonic dark matter. While the simplest hidden sectors in each case may consist of a single state, various extensions have been explored in recent years, motivated by specific experimental anomalies. In particular, these extensions allow for models of dark matter with enhanced or suppressed interaction rates or sub-weak scale masses.

From a general perspective, we would expect leading couplings to a neutral hidden sector to arise through relevant and marginal interactions. There are only three such flavor-universal 'portals' in the SM: the relevant interaction of the Higgs with a scalar operator $\mathcal{O}_S H^\dagger H$; the right-handed neutrino coupling LHN_R; and the kinetic mixing of a new U(1) vector V_μ with hypercharge $B_{\mu\nu}V^{\mu\nu}$. Of these, the latter vector portal is of particular interest as it leads to bilinear mixing with the photon and thus is experimentally testable, and at the same time allows for a vector which is naturally light. This portal has been actively studied in recent years, particularly in the 'dark force' regime in which the vector is a loop factor lighter than the weak scale, $m_V \sim$ MeV–GeV [1].

The model for this hidden sector is particularly simple. Besides the usual kinetic and mass terms for V, the coupling to the SM is given by [2]

$$\mathcal{L}_{\rm V} = -\frac{\kappa}{2} F_{\mu\nu} V^{\mu\nu} = e\kappa V_\mu J^\mu_{\rm em}. \tag{1}$$

Thus all phenomenological consequences of the model, including the production and decay of new vectors, are regulated by just two parameters, κ and m_V. This makes the model a very simple benchmark for all light, weakly interacting, particle searches. There are, however, options with regard to the origin of the mass of V, either a new Higgs mechanism, or m_V as a fundamental parameter—the so-called Stueckelberg mass. In this paper, we will concentrate on the latter option for simplicity.

The SM decay channels of V are well known. In the mass range where hadronic decays are important, one can use direct experimental data for the R ratio to infer couplings to virtual timelike photons, and hence to determine the decay rate Γ_V and all the branching ratios. In a wide mass range from $\sim 1 - 220\,$MeV, the vector V decays purely to electron-positron pairs with lifetime

$$\tau_V \simeq \frac{3}{\alpha_{\rm eff} m_V} = 6 \times 10^5 \text{ yr} \times \frac{10 \text{ MeV}}{m_V} \times \frac{10^{-35}}{\alpha_{\rm eff}} \tag{2}$$

where we have introduced the effective electromagnetic fine structure constant, absorbing the square of the mixing angle into its definition,

$$\alpha_{\rm eff} \equiv \alpha\kappa^2. \tag{3}$$

Importantly, we assume no light hidden sector states χ charged under U(1), so that there are no "dark decays" of $V \to \chi\bar{\chi}$ that would erode the visible modes and shorten the lifetime of V.

The normalization of the various quantities in (2) roughly identifies the region of interest in the $\{\kappa, m_V\}$ parameter space for this paper. We will explore the cosmological consequences of these hidden U(1) vectors with masses in the MeV-GeV range, and lifetimes long enough for the decay products to directly influence the physical processes in the Universe following BBN, and during the epoch of CMB decoupling. These vectors have a parametrically small coupling to the electromagnetic current, and thus an extremely small production cross sections for $e^+e^- \to V\gamma$,

$$\sigma_{\rm prod} \sim \frac{\pi\alpha\alpha_{\rm eff}}{E^2_{\rm c.m.}} \sim 10^{-66}\text{–}10^{-52}\ {\rm cm}^2, \tag{4}$$

where we took $E_{\rm c.m.} \sim 200$ MeV and the range is determined by our region of interest,

$$\alpha_{\rm eff} \sim 10^{-38}\text{–}10^{-24}. \tag{5}$$

Such small couplings render these vector states completely undetectable in terrestrial particle physics experiments, and consequently we refer to them as *very dark photons* (VDP). As follows from the expression (2) for the lifetime, the lower limit of the above range for $\alpha_{\rm eff}$ is relevant for CMB physics, while the upper limit is important for BBN.

The production cross section (4) looks prohibitively small, but in the early Universe at $T \sim m_V$ every particle in the primordial plasma has the right energy to emit V's. The cumulative effect of early universe production at these temperatures, followed by decays at $t \sim \tau_V$, can still inject a detectable amount of electromagnetic energy. A simple parametric estimate for the electromagnetic energy release per baryon, omitting $\mathcal{O}(1)$ factors, takes the form

$$E_{\rm p.b.} \sim \frac{m_V\Gamma_{\rm prod}H^{-1}_{T=m_V}}{n_{b,T=m_V}} \sim \frac{\alpha_{\rm eff}M_{\rm Pl}}{10\eta_b} \sim \alpha_{\rm eff} \times 10^{36}\ {\rm eV}. \tag{6}$$

Here the production rate per unit volume, $\Gamma_{\rm prod}$, was taken to be the product of the typical number density of particles in the primordial plasma and the V decay rate, $\tau_V^{-1}n_{\gamma,T=m_V}$. This production rate is active within one Hubble time, $H^{-1}_{T=m_V}$, leading to the appearance of the Planck mass in (6), along with another large factor, the ratio of photon to baryon number densities, $\eta_b^{-1} = 1.6 \times 10^9$. One observes that the combination of these two factors is capable of overcoming the extreme suppression by $\alpha_{\rm eff}$. Given that BBN can be sensitive to an energy release as low as O(MeV) per baryon, and that the CMB anisotropy spectrum allows us to probe sub-eV energy injection, we reach the conclusion that the early universe can be an effective probe of VDP. The cosmological signatures of the decaying VDP were partially explored in [3,4], but to our knowledge the CMB constraints on this model were not previously studied.

In the remainder of this paper, we provide detailed calculations to delineate the VDP parameter regions that are constrained by BBN and CMB data. In the process, we provide in Sec. II an improved calculation of the freeze-in abundance in the early universe (using some recent insight about the in-medium production of dark vectors [5,6]; see also [7]). In Sec. III, we explore the BBN constraints in more detail, including the speculative possibility that the currently observed over-abundance of ^{7}Li can be reduced via VDP decays. Then in Sec. IV we consider the impact of even later decays on the CMB anisotropies. A summary of the constraints we obtain is shown in Fig. 1, and more detailed plots of the parameter space are shown in Secs. III and IV. We finish with some concluding remarks in Sec. V. Several Appendices contain additional calculational details.

II. FREEZE-IN ABUNDANCE OF VDP

The cosmological abundance of long-lived very dark photons is determined by the freeze-in mechanism. While there are several possible production channels, the simplest and most dominant is the inverse decay process. When quark (or more generally hadronic) contributions can be neglected, the inverse decay proceeds via coalescence of $e^\pm$ and $\mu^\pm$, $l\bar{l} \to V$, shown in Fig. 2.

The Boltzmann equation for the total number density of V takes the form

$$\dot{n}_V + 3\,Hn_V = \prod_{i=l,\bar{l},V}\int\left(\frac{d^3\mathbf{p}_i}{(2\pi)^3 2E_i}\right) N_l N_{\bar{l}} \times (2\pi)^4\delta^{(4)}(p_l + p_{\bar{l}} - p_V)\sum|M_{l\bar{l}}|^2, \tag{7}$$

where the right hand side assumes the rate is sub-Hubble so that V never achieves an equilibrium density. The product of Fermi-Dirac (FD) occupation numbers, $N_{l(\bar{l})} = [1 + \exp(-E_{l(\bar{l})}/T)]^{-1}$, is usually considered in the Maxwell-Boltzmann (MB) limit, $N_l N_{\bar{l}} \to e^{(E_l+E_{\bar{l}})/T}$. Although this is not justified parametrically, numerically the FD $\to$ MB substitution is quite accurate, because as it turns out the peak in the production rate (relative to entropy) is at $T < m_V$ [3].

The matrix element $\sum|M_{l\bar{l}}|^2$ is summed over both initial and final state spin degrees of freedom. In general, it should

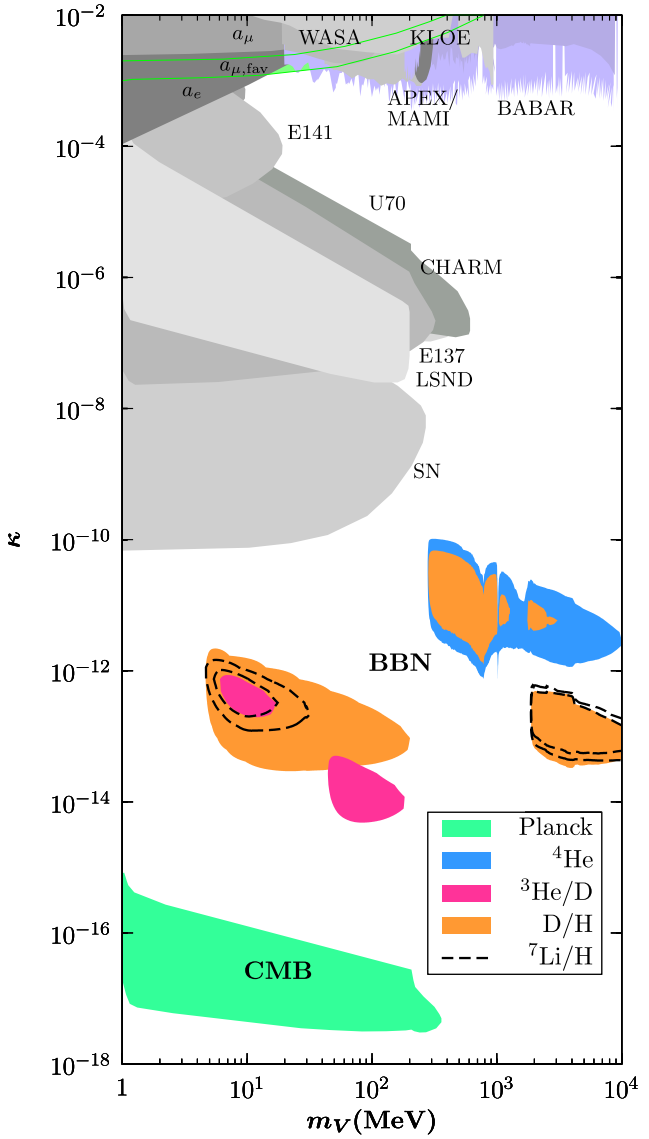

FIG. 1 (color online). An overview of the constraints on the plane of vector mass versus kinetic mixing, showing the regions excluded due to their impact on BBN and the CMB anisotropies, in addition to various terrestrial limits [1,8], including the more recent limits [9]. These excluded regions are shown in more detail in later sections.

include the in-medium photon propagator in the thermal bath, and the fermion wave functions. Among these modifications the most important ones are those that lead to the resonant production of dark photon states. However, resonant production occurs at much earlier times [3], at temperatures $T_r^2 \geq 3m_V^2/(2\pi\alpha) \simeq (8m_V)^2$, and turns out to be parametrically suppressed relative to continuum production; the details of the corresponding calculation are included in Appendix A. The dominant continuum production corresponds to temperatures of m_V and below where the T-dependence of $\sum|M_{l\bar{l}}|^2$ can be safely neglected. In the present model it is given by

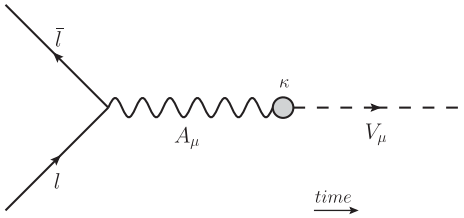

FIG. 2. Illustration of the coalescence production of the dark photon V via an off-shell photon.

$$\sum|M_{l\bar{l}}|^2 = 16\pi\alpha_{\mathrm{eff}}m_V^2\left(1+2\frac{m_l^2}{m_V^2}\right). \tag{8}$$

The same matrix element determines the decay width,

$$\Gamma_{V\to l\bar{l}} = \frac{\alpha_{\mathrm{eff}}}{3}m_V\left(1+2\frac{m_l^2}{m_V^2}\right)\sqrt{1-4\frac{m_l^2}{m_V^2}}. \tag{9}$$

The right hand side of (7), that can be understood as the number of V particles emitted per unit volume per unit time. In the MB approximation, it can be reduced to

$$\frac{1}{(2\pi)^3}\frac{1}{4}\int_{\mathrm{Eq.\ 11}} dE_l dE_{\bar{l}} e^{-\frac{E_l+E_{\bar{l}}}{T}}\sum|M_{l\bar{l}}|^2, \tag{10}$$

where the integration region is given by

$$\left|\frac{m_V^2}{2}-m_l^2-E_lE_{\bar{l}}\right| \leq \sqrt{E_l^2-m_l^2}\sqrt{E_{\bar{l}}^2-m_l^2}. \tag{11}$$

In the approximation where only electrons are allowed to coalesce and their mass neglected, $m_l \ll m_V < 2m_\mu$, (11) reduces to $E_lE_{\bar{l}} \geq m_V^2/4$ and the integration leads to the familiar modified Bessel function,

$$s\dot{Y}_V = \dot{n}_V + 3Hn_V = \frac{3}{2\pi^2}\Gamma_{V\to l\bar{l}}m_V^2TK_1(m_V/T), \tag{12}$$

where $Y_V = n_V/s$ is the number density normalized by the total entropy density, and $\Gamma_{V\to l\bar{l}} = \alpha_{\mathrm{eff}}m_V/3$, without (m_l^2/m_V^2)-suppressed corrections, is used for consistency. The final freeze-in abundance via a given lepton pair is given by

$$Y_{V,f}^l = \int_0^\infty dT\frac{\dot{Y}_V^l}{H(T)T}. \tag{13}$$

The integrals are evaluated numerically using

$$H(T) \simeq 1.66\sqrt{g_*(T)}\frac{T^2}{M_{\mathrm{pl}}}; \qquad s(T) = \frac{2\pi^2}{45}g_*(T)T^3, \tag{14}$$

where $g_*(T)$ is the effective number of relativistic degrees of freedom, evaluated with the most recent lattice and perturbative QCD results (see Appendix A for details).

For the simplest case of the MB distribution, with only relativistic electrons and positrons contributing and away from particle thresholds that change $g_*(T)$, the final integral can be evaluated analytically, and we have

$$Y^e_{V,f} = \frac{9}{4\pi}\frac{m_V^3\Gamma_{V\to e\bar{e}}}{(Hs)_{T=m_V}} = 0.72\frac{m_V^3\Gamma_{V\to e\bar{e}}}{(Hs)_{T=m_V}}. \quad (15)$$

This number reduces somewhat if the FD statistics is used, $0.72_{\rm MB} \to 0.54_{\rm FD}$, but receives a $\sim$20% upward correction from the transverse resonance (see Appendix B). Our numerical integration routine includes both the correct statistics and the addition of resonant production.

While the treatment of leptonic VDP production might be tedious but straightforward, hadronic production in the early universe is not calculable in principle, as one cannot simply extrapolate measured rates for the conversion of virtual photons to hadrons above temperatures of the QCD and/or chiral phase transitions. While the generic scaling captured by Eq. (15) holds, one needs to make additional assumptions about the treatment of the primordial hadron gas. It seems reasonable to assume that at high temperatures, when all light quarks are deconfined, the individual quark contribution $Y^q_{V,f}$ can be added by imposing a lower cutoff at the confinement scale T_c in the integral (13) and multiplying the matrix element (8) by the square of the quark electric charge Q_q^2. Below T_c we will use a free meson gas as an approximation for the hadronic states, and production via inverse charged pion and kaon decays $\{\pi^+\pi^-, K^+K^-\} \to V$ is included using a scalar QED model (see Appendix C).

The VDPs when produced are semirelativistic, and the subsequent expansion of the Universe quickly cools them so that at the time of decay $E_V = m_V$. The decay deposits this energy into $e^\pm$, $\mu^\pm$ and $\pi^\pm$ pairs, and more complicated hadronic final states when m_V is above the ρ resonance. Thus, the energy stored per baryon (before the characteristic decay time) is given by

$$E_{\rm p.b.} = m_V Y_{V,f}\frac{s_0}{n_{b,0}}, \quad (16)$$

where $n_{b,0}/s_0 = 0.9\times10^{-10}$ is the baryon-to-entropy ratio today. $E_{\rm p.b.}$ is shown in two separate panels in Fig. 3. The top panel shows it as a function of m_V at fixed $\alpha_{\rm eff}$, and the lower panel fixes the VDP lifetime to $\tau_V = 10^{14}$ s. We illustrate the contributions from the different production channels. Using this calculated VDP energy reservoir we are now ready to explore its consequences for BBN and the CMB.

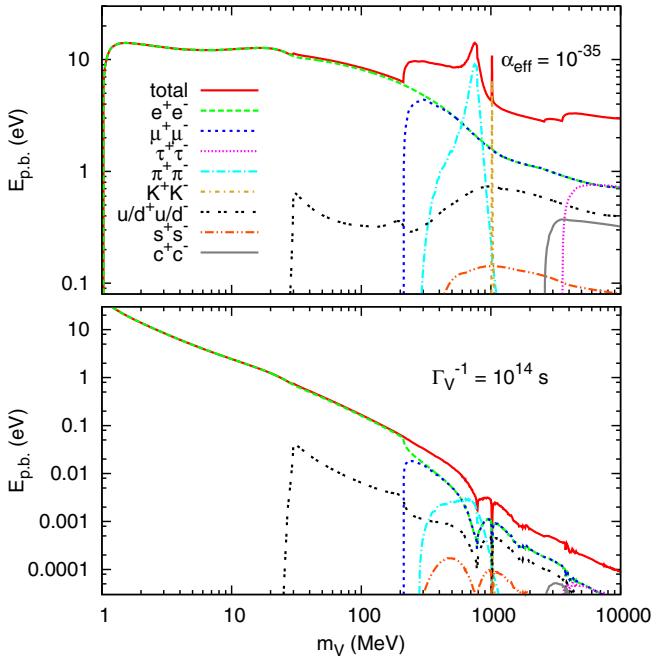

FIG. 3 (color online). Total energy stored per baryons for $\alpha_{\rm eff} = 10^{-35}$ (upper) and $\Gamma_V^{-1} = 10^{14}$ s (lower) from the various production channels as labeled.

III. IMPACT ON BBN

Late decays of dark photons affect the epoch of primordial nucleosynthesis after cosmic time $t \gtrsim 1$ s in a variety of ways. The resulting constraints are governed by a combination of lifetime and abundance, and both have complementary trends with respect to m_V; $\tau_V(Y_V)$ decreases (increases) with growing mass. Therefore we generally expect constraints to be bounded and localized islands in parameter space with the relevant combination of m_V and Y_V to ensure BBN sensitivity.

Prior to decay, V contributes to the matter content substantially, $n_V/n_b \lesssim 10^8$ for $\tau_V < 1$ s. Whereas the modification of the Hubble rate is generally small, the decays of V imply the injection of electrons, muons, pions, etc., in numbers larger than baryons. The effects on BBN are best described by partitioning the decay into electromagnetic and hadronic energy injection and in the following we provide a lightning review of those modes separately.

MeV-scale dark photons with $m_V < 2m_\pi$ provide a prototypical model of electromagnetic energy injection because the dominant kinematically accessible decay modes are $V \to e^+e^-, \mu^+\mu^-$. Muons decay before interacting weakly, and electron-positron pairs are instantly thermalized via rapid inverse Compton scattering on background photons. An electromagnetic cascade forms in energy degrading interactions of photons and electrons. The large number of photons created gives rise to a nonequilibrium destruction and creation of light elements.

The most important feature of the injected photon energy spectrum $f_\gamma(E_\gamma)$ is a sharp cut-off for energies above the $e^\pm$ pair-creation threshold on ambient photons, $E_{\rm pair} \simeq m_e^2/(22T)$. High-energy photons are efficiently dissipated before they can interact with nuclei, so that to good approximation $f_\gamma(E_\gamma) = 0$ for $E_\gamma > E_{\rm pair}$. In contrast, less

energetic photons below the pair-creation threshold can interact with the light elements. Equating $E_{\rm pair}$ against the thresholds for dissociation of the various light elements informs us about the temperature and hence cosmic time $t_{\rm ph}$ at which to expect the scenario to be constrained,

$$t_{\rm ph} \simeq \begin{cases} 2\times10^4\ {\rm s}, & {}^7{\rm Be}+\gamma\to{}^3{\rm He}+{}^4{\rm He} \quad (1.59\ {\rm MeV}), \\ 5\times10^4\ {\rm s}, & {\rm D}+\gamma\to n+p \quad (2.22\ {\rm MeV}), \\ 4\times10^6\ {\rm s}, & {}^4{\rm He}+\gamma\to{}^3{\rm He/T}+n/p \quad (20\ {\rm MeV}), \end{cases}$$

where the binding energy of the nucleus against destruction has been given in brackets. Finally, note that we also find that neutrino injection from muon decay does not yield observable changes in the light element abundances—a fascinating story in itself [4].

Once $m_V > 2m_\pi$, the hadronic channels open in the decay of V and the effects on BBN become more difficult to model. A major simplification is that only long-lived mesons $\pi^\pm$, $K^\pm$, and K_L, with lifetime $\tau \sim 10^{-8}$ s, and (anti-)nucleons have a chance to undergo a strong interaction reaction with ambient protons and nuclei. The relevant reactions are charge exchange, *e.g.* $\pi^- + p \to \pi^0 + n$, and absorption with subsequent destruction of light elements, *e.g.* $\pi^- + {}^4{\rm He} \to T + n$. Prior to the end of the deuterium bottleneck at $T \simeq 100$ keV only the former reactions are possible. They change the n/p ratio that determines the primordial ^{4}He value. Later, once elements have formed, charge exchange creates "extra neutrons" on top of the residual and declining neutron abundance. Moreover, spallation of ^{4}He with nonequilibrium production of mass-3 elements and secondaries, *e.g.* through ${\rm T} + {}^4{\rm He_{bg}} \to {}^6{\rm Li} + n$, are important. We model all such reactions in great detail, include secondary populations of pions from kaon decays, and various hyperon producing channels from reactions of kaons on nucleons and nuclei. A detailed exposition of the hadronic part along with a discussion of all included reactions can be found in our previous work [4]. More details are provided when discussing our findings below as well as in Appendix D.

We now proceed to review the light element observations that form the basis of our adopted limits. Probably the most notable recent developments in the determination of light element abundances are two precision measurements of D/H from high-z QSO absorption systems [10,11]. Both have error bars that are a factor ~5 smaller than the handful of previously available determinations. Taken together, the mean observationally inferred primordial D/H value now reads [11]

$${\rm D/H} = (2.53 \pm 0.04)\times10^{-5}. \tag{17}$$

Nonetheless, systematically higher levels of primordial D/H are conceivable, in spite of the above error bar. For example, D may be astrated or absorbed on dust grains. Indeed, values as high as 4×10^{-5} have been reported [12,13], so as a conservative upper limit we employ,

$${\rm D/H} < 3\times10^{-5}. \tag{18}$$

On the flip side, underproducing D yields a robust constraint since no known astrophysical sources of D exist. We account for this constraint either by adopting the nominal lower 2σ-limit from (17) or by demanding,

$${}^3{\rm He/D} < 1. \tag{19}$$

The latter limit employs the solar system value [14] and arises from the consideration that D is more fragile than ^{3}He, and hence a monotonically increasing function of time. Despite the uncertain galactic chemical evolution of ^{3}He, (19) can therefore be considered robust.

The inference of the primordial mass fraction Y_p from extragalactic H-II regions proved to be systematically uncertain in the past [15,16] and values in the range

$$0.24 \le Y_p \le 0.26 \tag{20}$$

have been reported. We adopt this range as our cosmologically viable region.

Finally, what is believed to be the primordial value of ^{7}Li/H, the so-called Spite plateau [17], is a factor of 3–5 lower than the lithium yield from standard BBN, ${}^7{\rm Li/H} = (5.24^{+0.71}_{-0.67})\times10^{-10}$ [18]. We deem the lithium problem solved in this model if we can identify a region in parameter space where lithium is reduced to the Spite plateau value,

$$10^{-10} < {}^7{\rm Li/H} < 2.5\times10^{-10}. \tag{21}$$

We take an opportunity to comment that the status of the lithium problem is somewhat controversial: while it is possible that new physics is responsible for its solution, the astrophysical lithium depletion mechanisms can also be invoked (see Ref. [19] for a review of this subject).

We are now in a position to present our results in Fig. 4 where a scan over the m_V, κ parameter space is shown, and contours of constant lifetime, τ_V and relic abundance n_V/n_b prior to decay are shown by the diagonal solid and dotted lines, respectively. Three distinct regions labeled I–III are identified as being in conflict with observations. They arise from distinct physical processes which we now proceed to describe.

Regions I: In the regions labeled I the dark photon exclusively decays to e^+e^-. They are associated with pure electromagnetic energy injection.

In region Ia with a ballpark lifetime $\tau_V \sim 10^5$ s, ^{7}Be and D are destroyed. From the outer to the inner (black) dashed curves, the ^{7}Li/H abundance is reduced to 4×10^{-10} and 3×10^{-10}, respectively. It is therefore a region in which the cosmological lithium problem is ameliorated. Smaller abundances of ^{7}Li/H are disfavored by the constraint ${}^3{\rm He/D} < 1$ (pink shaded region); an equivalent region from the requirement ${\rm D/H} > 10^{-5}$ coincides with this one

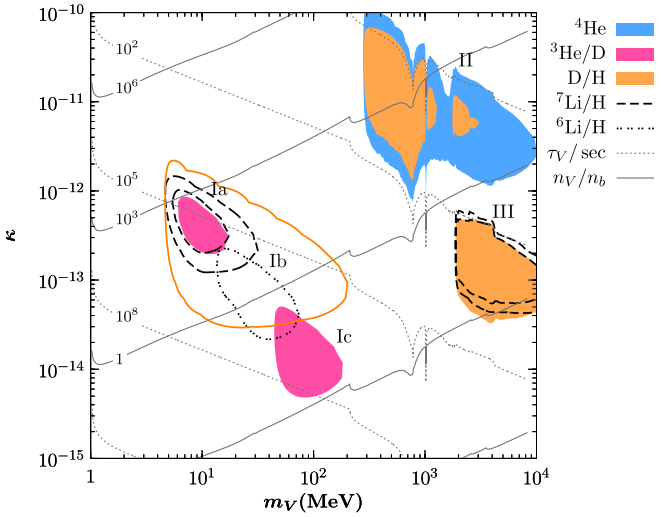

FIG. 4 (color online). Effects on BBN from the decay of relic dark photons as a function vector mass of m_V and kinetic mixing parameter κ. The diagonal gray lines are contours of lifetime τ_V (solid) and abundance per baryon n_V/n_b prior to decay (dotted). Shaded regions are excluded as they are in conflict with primordially inferred light element abundances. The solid (orange) closed line is a potential 2σ constraint from underproduction of D/H derived from (17). The dashed black lines are contours of decreasing ^{7}Li/H abundance, 4×10^{-10} and 3×10^{-10}, going from the outside to the inside, respectively. The dotted line shows $^6\mathrm{Li/H} = 10^{-12}$ which corresponds to an extra production by about two orders magnitude but without being in conflict with observations.

and is not shown. If we take the new measurements (17) at face value, the prospective solution to the lithium problem is excluded altogether by the nominal 2σ lower limit on D/H shown by the (orange) solid closed line.

In region Ib, in addition to the potential underproduction of D/H, photodissociation of ^{7}Li and ^{7}Be leads to the primary production of $^6\mathrm{Li/H} > 10^{-12}$. This is not at the level of a constraint, but we show the dotted contour anyway in order to better illustrate what is happening in the respective regions of parameter space.

Finally, in region Ic, with V-lifetime of $\sim 10^7$ s, ^{4}He is being dissociated and the net creation of ^{3}He/D rules out this region of parameter space. Once ^{4}He is split, ^{6}Li can be produced through a secondary mechanism of energetic mass-3 spallation products such as $\mathrm{T} + {}^4\mathrm{He}|_{\mathrm{bkg}} \to {}^6\mathrm{Li} + n$. We find, however, that such channels are not efficient enough to provide any additional constraint.

Region II: Now we turn to the low-lifetime/high-abundance region II. The lifetime of V is below 100 s and hence marks a choice of parameters where the dark photon decays before the end of the D-bottleneck ($T \sim 100$ keV). The injection of pions and—if kinematically allowed—of kaons and nucleons, induces $n \leftrightarrow p$ interconversion. It has the general effect that the n/p-ratio rises. The elevated number of neutrons that in turn become available at the end of the D-bottleneck allow for more D-formation and subsequently more ^{4}He. The region is therefore challenged by the constraints $Y_p \leq 0.26$ and $\mathrm{D/H} \leq 3 \times 10^{-5}$.

Region III: Finally, region III is characterized by the presence of "extra neutrons" that appear right after the main stage of nucleosynthesis reactions at cosmic times $t \sim 10^3$ s. The origin of those neutrons is twofold. First, there is a direct injection of n from the decay $V \to n\bar{n}$. Second, there is indirect production, from charge exchange of π^- on protons, $\pi^- p \to n\pi^0$ or $\pi^- p \to n\gamma$, and from hyperon production by "s-quark" exchange of K^- on protons with subsequent hyperon decay. We note in passing that $K^- p \to \bar{K}^0 n$ has positive Q-value and is not allowed for stopped kaons; conservatively, we neglect this reaction.

The elevated neutron abundance leads to a chain of reactions that depletes the overall lithium abundance,

$$\text{step 1:}\ {}^7\mathrm{Be} + n \to {}^7\mathrm{Li} + p, \tag{22}$$

$$\text{step 2:}\ {}^7\mathrm{Li} + p \to {}^4\mathrm{He} + {}^4\mathrm{He}. \tag{23}$$

In the first step, ^{7}Be charge exchanges with the neutron and forms ^{7}Li. In a second step, ^{7}Li, because it has one less unit of charge, is more susceptible to being destroyed by protons. The result of this mechanism is shown in Fig. 4 by the dashed curves. Most of the extra neutrons are, however, intercepted by protons so that this potential solution to the lithium problem is always accompanied by an elevated D-yield. The D/H constraint (18) is shown by the (orange) solid region.

A more detailed description of the calculations used to obtain these results is provided in Appendix D.

IV. IMPACT ON THE CMB

Later decays of VDP, which occur after recombination if $\tau_V \gtrsim 10^{13}$ s, can leave an imprint on the CMB. In particular, as discussed in [20,21], the altered ionization history tends to enhance the TE and EE spectra on large scales, while the TT temperature fluctuation is damped on small scales. Consequently, precision CMB data can be used to further constrain the VDP parameter space in regimes where the late decays impact the ionization history.

The energy injection of a decaying species can be generically parametrized as [20,21]

$$\frac{dE}{dtdV} = 3\zeta m_{\mathrm{p}} \Gamma e^{-\Gamma t}, \tag{24}$$

with $(1 - x_e)/3$ of this energy going to ionization and $(1 + 2x_e)/3$ heating the medium, x_e representing the ionized fraction. The energy output of each decay is $3\zeta m_{\mathrm{p}}$, the normalization chosen so that (24) gives the ionizing energy after recombination ($x_e \to 0$). Using CLASS [22] to obtain the CMB power spectra and MONTEPYTHON [23] as a Monte Carlo Markov Chain driver, we determine the 2σ

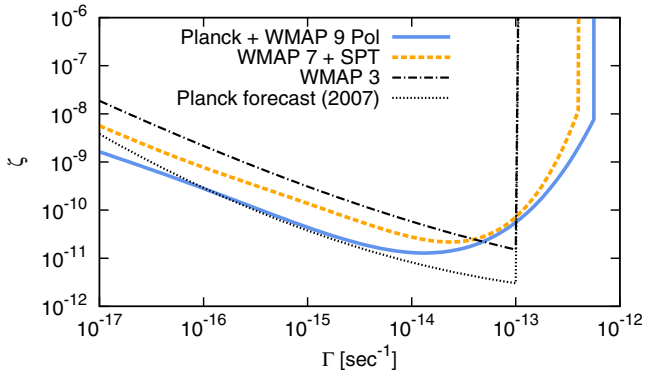

FIG. 5 (color online). CMB constraints on the energy injection parameters ζ and Γ. For comparison, we include the WMAP3 curve and the Planck forecast (2007) from Ref. [21].

limits from the Planck 2013 results [24] (which also incorporates the low-l polarization likelihood from WMAP9 [25]). The limits are shown in Fig. 5, with constraints similarly derived from WMAP7 [26] +SPT [27], along with the WMAP3 and 2007 Planck forecast fits from [21]. The cutoff at $\Gamma^{-1} = 10^{13}$ s appears since Ref. [21] used a purely matter-dominated approximation for the elapsed time $[t(z) \sim (1+z)^{-3/2}]$ in the exponential of (24) and assumed that decay lifetimes shorter than 10^{13} seconds happen before recombination and do not impact the CMB. In our calculations, we use the exact time from ΛCDM cosmology and obtain a more accurate picture for shorter lifetimes.

The energy output ζ can be related to the VDP parameters as follows,

$$\zeta = \frac{f}{3}\frac{\Omega_V}{\Omega_b} = \frac{f}{3}\frac{E_{\text{p.b.}}}{m_p}. \tag{25}$$

The prefactor f determines the overall efficiency with which the deposited energy goes into heating and ionization. The thermalization of an energetic particle depends on the species, initial energy and redshift [28,29]. Ref. [30] provides transfer functions $T(z_{\text{inj}}, z_{\text{dep}}, E)$ giving the fractional amount of energy deposited at z_{dep} for an energy injection E at z_{inj} for both γ and e^+e^- final states. With this information, we can numerically solve for the deposition efficiency of the injected energy from decaying particles [30],

$$f(z) = \frac{\frac{dE}{dz}|_{\text{dep}}(z)}{\frac{dE}{dz}|_{\text{inj}}(z)} \tag{26}$$

$$= \frac{H(z)\sum_{\text{species}}\int_z^\infty \frac{d\ln(1+z_{\text{in}})}{H(z_{\text{in}})}\int T(z_{\text{in}}, z, E) E \frac{d\tilde{N}}{dE} dE}{\sum_{\text{species}}\int E\frac{d\tilde{N}}{dE}dE}, \tag{27}$$

where $\frac{d\tilde{N}}{dE}$ is the normalized energy distribution of the e^+e^- or γ in the decaying particle rest frame. This strategy has been

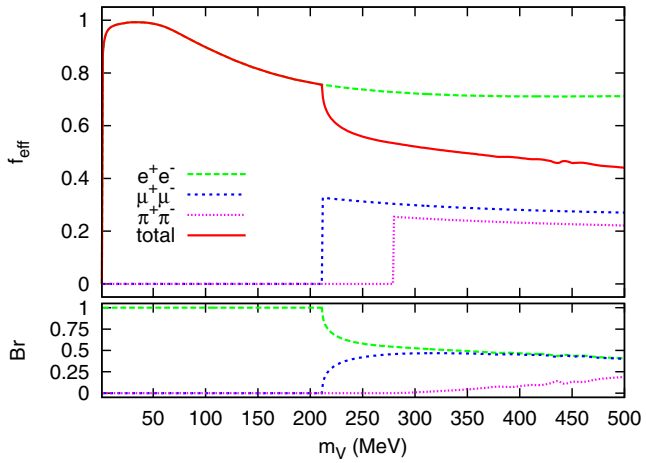

FIG. 6 (color online). Effective deposition efficiency for each decay channel with the sum weighted by the branching ratios for $\Gamma_V^{-1} = 10^{14}$ s.

used in Refs. [28,31] to analyze dark matter annihilation and decay to standard model particles for $m_\chi > 1$ GeV. An effective deposition efficiency f_{eff} is found by averaging $f(z)$ over the range $800 < z < 1000$. We compute f_{eff} for VDP in the mass range 1–500 MeV where the decay channels are $V \to \{e^+e^-, \mu^+\mu^-, \pi^+\pi^-\}$ [32]. The results for $f_{\text{eff}}(m_V)$, along with each decay channel contributions and their branching ratios, are shown in Fig. 6 for $\Gamma_V^{-1} = 10^{14}$ s. The low efficiency of $\mu^\pm$ and $\pi^\pm$ is due to the neutrinos radiating away a large fraction of the energy. For $e^\pm$ with $E \gtrsim 100$ MeV, the longer cooling time lowers the efficiency [30], which is clearly seen in the $f_{\text{eff}}^{e^\pm}$ curve.

Using the result (16) with f_{eff} in (25), we find that our CMB constraints on $\Gamma - \zeta$ lead to the excluded region of parameter space shown in Fig. 7. We find this to be a rather remarkable sensitivity to an effective electromagnetic coupling as small as $\alpha_{\text{eff}} \sim 10^{-37}$–$10^{-38}$.

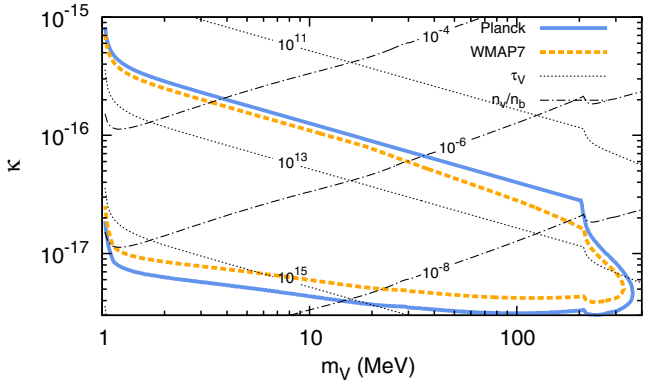

FIG. 7 (color online). The solid contours bound the regions excluded by the CMB constraints on VDP. Contours of the lifetime in seconds and relative number density of dark photons to baryons prior to their decay are also shown.

V. CONCLUDING REMARKS

The kinetic mixing portal is one of the few renormalizable interaction channels between the SM and a neutral hidden sector. As such, it is of interest to understand the full spectrum of limits on dark photons coupled through this portal. In this paper, we have determined the cosmological constraints due to the impact of late decays on BBN and the CMB; the sensitivity extends to remarkably small effective electromagnetic couplings. In this concluding section, we comment on possible indirect signatures in the present-day universe from the decay of relic dark photons, and other potential extensions.

It is important to emphasize that the constraints derived in this work rely only on the thermal production of VDP and the minimal cosmological history of the Universe. For the mass range of VDP considered here, the constraints will hold as long as temperatures $T \sim \mathcal{O}(1)$–$\mathcal{O}(100)$ MeV were attained at an early epoch. Any additional contributions to the abundance of VDP, such as production of V through other portals, or nonthermal contributions to $m_V^2\langle V_\mu^2\rangle$ due to vacuum misalignment mechanisms, will enhance the VDP abundance, and correspondingly strengthen the bounds on κ.

The analysis in this paper assumed that the vector mass was above the electron threshold. For lower masses, V naturally has a lifetime well in excess of the age of the Universe and can play the role of dark matter [3,33]. In this regime its relic abundance is fixed instead by Thomson-like scattering, $e + \gamma \to e + V$. As discussed in [33], for $m_V \sim 100$ keV, indirect constraints still allow this cosmological abundance with $\kappa \sim 10^{-11}$, but photoelectric absorption in dark matter detectors would leave a detectable ionization signal. The electronic background data from XENON100 in the 1–100 keV range [34] indicated no signal, thus appearing to close this window, as discussed in more detail in [35]. Very recently, these limits have also been improved by XMASS [36]. Nevertheless, minimal extensions of VDP in this mass range can provide viable models of superweakly interacting massive particle dark matter. One option is to have a dark Higgs h' responsible for breaking $U(1)_V$ and generating the dark photon mass. In the $m_{h'} < m_V$ regime, this will lead to extremely long-lived h' particle states since $\Gamma_{h'} \propto \kappa^2$ [32]. In this case, one would require somewhat larger values of κ to ensure a more efficient $e^-e^+ \to Vh'$ production channel. Another option is simply a new state state χ, which is stable and charged under V. The analysis of these very light dark matter models goes beyond the scope of the present paper.

We can also consider a higher mass range, e.g. TeV-scale dark photons, whose present-day decays could provide signatures in antimatter, gamma-ray and neutrino observations [37]. With a more massive dark vector, the full kinetic mixing with hypercharge should be included, $\mathcal{L}_V = -\frac{\tilde{\kappa}}{2}B_{\mu\nu}V^{\mu\nu} = -\frac{\kappa}{2}F_{\mu\nu}V^{\mu\nu} + \frac{\kappa\tan\theta_w}{2}B_{\mu\nu}Z^{\mu\nu}$, where $\tilde{\kappa} = \kappa\cos\theta_w$ to keep the same normalization as before. Fermions then acquire both vector and axial vector couplings to V, modifying both the production and decays rates. Assuming $m_V \gg m_Z$, and generalizing (8) by summing over all degrees of freedom for γ and Z mediation, leads to

$$\Gamma_V \simeq 10^{-17}\ \mathrm{s}^{-1}\left(\frac{\alpha_{\mathrm{eff}}}{10^{-45}}\right)\left(\frac{m_V}{1\ \mathrm{TeV}}\right). \tag{28}$$

In the MB approximation, freeze-in production is analogous to (15), and using $g_\star \simeq 100$ and summing over the channels, we find

$$Y_{V,f} \simeq 10^{-31}\left(\frac{\Gamma_V}{10^{-17}\ \mathrm{s}^{-1}}\right)\left(\frac{\mathrm{TeV}}{m_V}\right)^2. \tag{29}$$

This is minuscule compared to the cold dark matter energy density,

$$\frac{n_V m_V}{\rho_{\mathrm{CDM}}} \simeq 10^{-19}\left(\frac{\Gamma_V}{10^{-17}\ \mathrm{s}^{-1}}\right). \tag{30}$$

Decaying dark matter of that mass range, with 100% leptonic branching, requires a lifetime of $\tau_{\mathrm{DM}} = 10^{26}$ s [37] to contribute to the increasing positron fraction in cosmic rays observed by PAMELA [38] and AMS-02 [39]. The VDP scenario thus falls short by many orders of magnitude. Similar conclusions follow for neutrino experiments, where decaying dark matter with mass 10–10^{15} TeV requires a lifetime of $\mathcal{O}(10^{26}$–$10^{28})$ s [40,41]. Very long-lived dark photons are therefore too feebly coupled in this minimal scenario to contribute to these indirect detection signals.

Finally, we note that the analysis performed in this paper can easily be extended to other cases of "very dark" particles. For example, super-weakly interacting singlet scalars S, coupled to the SM via the renormalizable Higgs portals $ASH^\dagger H + \lambda S^2 H^\dagger H$ can be probed via BBN [4] and the CMB. While the main cosmological constraints will be very similar to the VDP case, the details of the production from the Higgs portal are different, and shifted to the earlier electroweak epoch. The analysis of this minimal scalar model is ongoing [42].

ACKNOWLEDGMENTS

We would like to thank H. An, J. Redondo and D. Walker for helpful discussions. This work was supported in part by NSERC, Canada, and research at the Perimeter Institute is supported in part by the Government of Canada through NSERC and by the Province of Ontario through MEDT. The work of A. F is partially supported by the Province of Québec through FRQNT. J. P is supported by the New Frontiers program of the Austrian Academy of Sciences.

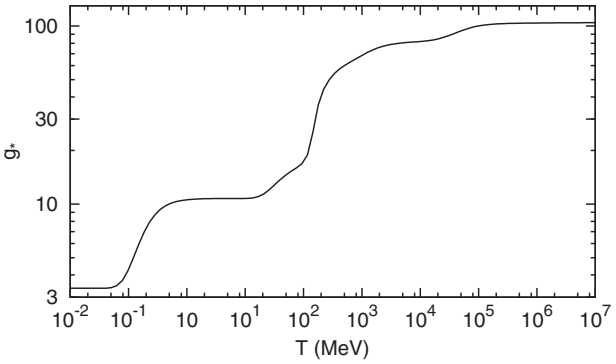

FIG. 8. Relativistic degrees of freedom as a function of temperature.

APPENDIX A: DEGREES OF FREEDOM

Our evaluation of the number of relativistic degrees of freedom needed in the Hubble rate and entropy density follows the technique used in [43], updated with more recent theoretical QCD results.

The BMW lattice QCD group [44] provides a fitting function for the trace anomaly, from which we can extract the energy and entropy density. Their function incorporates the hadron resonance gas model below the pseudocritical temperature T_c and $n_f = 2+1$ lattice results up to 1000 MeV. At higher temperatures, we used the $n_f = 3$ three-loop result from hard-thermal-loop perturbation theory [45] with renormalization scale $\Lambda = 2\pi T$. The heavier quarks are modelled as an ideal gas, scaled by the ratio of the energy density of $n_f = 3$ QCD to the ideal gas value at the given temperature. This approximation has been used in [43] and is shown to be in good agreement with preliminary lattice results for $n_f = 2+1+1$ [46]. The resulting $g_\star(T)$ is shown in Fig. 8.

The QCD phase transition is a crossover [47], with a pseudocritical temperature T_c in the range of 150–170 MeV. For a given observable, T_c is well defined as the temperature of the maximal inflection point. In the present work, we used $T_c = 157$ MeV, the pseudocritical temperature of the energy density [48].

APPENDIX B: RESONANT PRODUCTION

Here we demonstrate that the thermal effects, and the associated resonant production, create a parametrically suppressed contribution to $Y_{V,f}$, although numerically it may constitute as much as 30%.

1. Relativistic case

We begin the analysis by choosing the simplest case of electron-positron coalescence and use MB statistics. Since thermal effects are going to be important at higher temperatures than m_V, m_e is negligible and can be set to 0 from the start. Furthermore, we break up the matrix element into the longitudinal and transverse pieces according to the polarization of the V boson produced with four-momentum $(\omega, \vec{q})$ to derive the right-hand side of the Boltzmann equation (7). After direct calculation we obtain

$$\text{rhs} = \frac{3}{2\pi^2} m_V \Gamma_{V\to e\bar{e}} \int_{m_V}^{\infty} d\omega \sqrt{\omega^2 - m_V^2}\, e^{-\omega/T} \times \left\{ \frac{1}{3} \frac{m_V^4}{|m_V^2 - \Pi_L|^2} + \frac{2}{3} \frac{m_V^4}{|m_V^2 - \Pi_T|^2} \right\}. \tag{B1}$$

The polarization tensors $\Pi_{T(L)}$ are complex functions of $\omega, |\vec{q}|$ and T, and originate from the virtual photon propagators. In the limit of vanishing plasma density, $\Pi_{T(L)} \to 0$, the expression inside $\{\ldots\}$ tends to 1, and the rhs becomes identical to that of (12), as it should be. The expressions for $\Pi_{T(L)}$ can be found in the thermal field theory literature, and we use the results of [49], with the more symmetric definition of the longitudinal polarization tensor [5], $\Pi_L^{\text{this work}} = \frac{m_V^2}{\omega^2 - m_V^2} \Pi_L^{\text{Ref. [42]}}$.

For a one-component ultrarelativistic plasma (again neglecting muon and pion contributions etc.), the expressions for the real parts of the polarization tensors are given by [49]

$$\begin{aligned} \text{Re}\Pi_T(\omega) &= \omega_p^2 \frac{3\omega^2}{2\vec{q}^2} \left(1 - \frac{m_V^2}{\omega^2} \frac{\omega}{2|\vec{q}|} \log \frac{\omega + |\vec{q}|}{\omega - |\vec{q}|} \right), \\ \text{Re}\Pi_L(\omega) &= 3\omega_p^2 \frac{m_V^2}{\vec{q}^2} \left(\frac{\omega}{2|\vec{q}|} \log \frac{\omega + |\vec{q}|}{\omega - |\vec{q}|} - 1 \right), \end{aligned} \tag{B2}$$

where all the factors of $|\vec{q}|$ can be replaced with $\sqrt{\omega^2 - m_V^2}$. The plasma frequency of the electron-positron fluid is given by

$$\omega_p^2 = \frac{4\pi\alpha}{9} T^2. \tag{B3}$$

The imaginary parts of the polarization tensors are related to the massive photon decay rate in vacuum, $\Gamma_0 = \alpha m_V/3$,

$$\text{Im}\Pi_{T(L)} = -\Gamma_0 m_V (1 - \exp(-\omega/T)). \tag{B4}$$

(The VDP decay rate in vacuum is $\kappa^2\Gamma_0$ in this approximation.) Armed with these expressions, we can derive the conditions for a resonance, that is the point in $\{T, \omega\}$ where the denominator of (B1) is minimized,

$$\text{Re}\Pi_{T(L)}(\omega, T_{r,T(L)}) = m_V^2. \tag{B5}$$

The dependence of $T_{r,T(L)}(\omega)$ is plotted in Fig. 9. The most important point is that all resonance frequencies are parametrically larger than m_V, and there is a minimum frequency at which the resonance can happen,

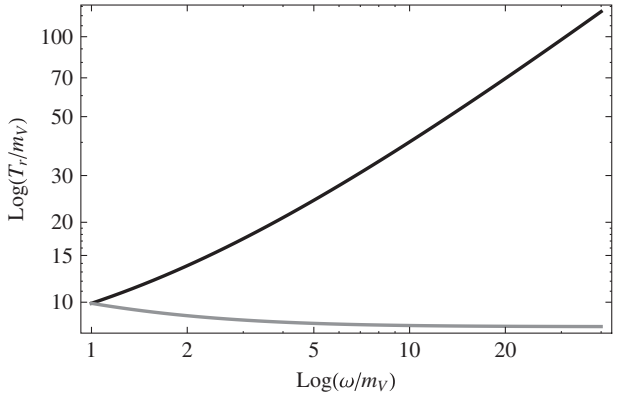

FIG. 9. The dependence of the resonant temperatures $T_{r,L}$ (black) and $T_{r,T}$ (gray) on frequency ω, all in units of m_V. The transverse resonance frequency asymptotes to $T_{\min} = m_V(3/(2\pi\alpha))^{1/2}$.

$$T_{\min} = m_V\left[\frac{3}{2\pi\alpha}\right]^{1/2} \simeq 8.1 m_V. \tag{B6}$$

Thus all resonances occur at temperatures that are parametrically larger (by a factor of $\alpha^{-1/2}$) than m_V, where the Hubble expansion rate is significantly greater than at $T < m_V$. We proceed by calculating the resonant contributions by using the narrow width approximation, that is we approximate the ratios inside the $\{\ldots\}$ of Eq. (B1) by delta functions,

$$\frac{m_V^4}{|m_V^2 - \Pi|^2} \simeq \frac{3\pi}{2\alpha}\frac{T_r(\omega)\delta[T - T_r(\omega)]}{e^{\omega/T} - 1}. \tag{B7}$$

This expression holds for both the T and L resonances.

The resonant contribution to the VDP abundance comes from evaluating two integrals, over T and ω. If the integral over the temperature is performed first, one finds

$$\Delta Y_{f,r} = Y_T + Y_L,$$
$$Y_{T(L)} = \frac{3 g_{T(L)}}{4\pi\alpha}\frac{m_V^3\Gamma_{V\to e\bar{e}}}{(Hs)_{T=m_V}}\int_{m_V}^{\infty}\frac{m_V^3\sqrt{\omega^2-1}\,d\omega}{(T_{r,T(L)}(\omega))^5[e^{\omega/T}-1]}, \tag{B8}$$

where $g_{T(L)} = 2(1)$ are the multiplicity factors. Performing the remaining integral we arrive at the following result,

$$\Delta Y_{f,r} \simeq \Delta Y_T \simeq 0.17 \times \frac{m_V^3\Gamma_{V\to e\bar{e}}}{(Hs)_{T=m_V}}. \tag{B9}$$

The longitudinal resonance turns out to be negligible on account of the large value of $T_{r,L}$ when $\omega \sim T_{r,L}$. (This is in contrast with the stellar production of very light dark photons, where the L resonance dominates [5].) We now see that although the resonant contribution (B9) is parametrically suppressed, by $O(\alpha^{1/2})$, relative to the continuum contribution (15), it can reach 20% of the total. Repeating the same calculations with FD statistics changes the coefficient only slightly, $0.17_{\rm MB} \to 0.15_{\rm FD}$.

2. Nonrelativistic corrections

The analytical treatment of resonant production above is only valid for massless particles in the loop. In our numerical calculations, we include the $\Pi_{T,L}$ effects for all leptons of mass $m < 10$ GeV and charged pions for $T < T_c$. Ref. [49] provides analytical approximations for $\mathrm{Re}\Pi_{T,L}$, which interpolate smoothly between the "classical" (nonrelativistic) and relativistic limits,

$$\mathrm{Re}\Pi_{\rm T} = \omega_p^2\frac{3}{2v_\star^2}\left(\frac{\omega^2}{k^2} - \frac{\omega^2 - v_\star^2 k^2}{k^2}\frac{\omega}{2v_\star k}\log\frac{\omega + v_\star k}{\omega - v_\star k}\right), \tag{B10}$$

$$\mathrm{Re}\Pi_{\rm L} = \omega_p^2\frac{3m_v^2}{v_\star^2 k^2}\left(\frac{\omega}{2v_\star k}\log\frac{\omega + v_\star k}{\omega - v_\star k} - 1\right), \tag{B11}$$

where

$$\omega_p^2 = \frac{8\alpha}{\pi}\int_0^\infty dp\,\frac{p^2}{E}\left(1 - \frac{1}{3}\frac{p^2}{E^2}\right)n_F(E), \tag{B12}$$

$$w_1^2 = \frac{8\alpha}{\pi}\int_0^\infty dp\,\frac{p^2}{E}\left(\frac{5}{3}\frac{p^2}{E^2} - \frac{p^4}{E^4}\right)n_F(E), \tag{B13}$$

$$v_\star = \frac{w_1}{w_p}. \tag{B14}$$

The parameter $v_\star$ can be interpreted as the typical velocity of the fermion at that given energy. We recover the relativistic limit (B2) with $v_\star \to 1$ and the "classical" (nonrelativistic) limit with $v_\star \to \sqrt{5T/m_f}$.

In general, the imaginary part of the polarization tensor is given by [50],

$$\mathrm{Im}\Pi = -\omega\Gamma^{\rm Prod}(e^{\frac{\omega}{T}} - 1), \tag{B15}$$

$$\Gamma^{\rm Prod} = \frac{1}{2\omega}\int\frac{d^3p}{2E_p}\frac{d^3q}{2E_1}\frac{(2\pi)^4}{(2\pi)^6}\delta^4(k - p - q) \tag{B16}$$

$$\times\,|\mathcal{M}_{1,2\to V}|^2 n_1 n_2. \tag{B17}$$

Here $\Gamma^{\rm Prod}$ represents the production rate, with $\mathcal{M}_{1,2\to V}$ the matrix element for the particles coalescing into V and n_1 and n_2 their respective statistical distributions. Separating the T and L parts of matrix element,

$$|\mathcal{M}^{T,L}_{l\bar{l}\to V}|^2 = 16\pi\alpha(F^T + F^L), \tag{B18}$$

$$F^T = -2p^2\sin^2\theta + m_V^2, \tag{B19}$$

$$F^L = -\frac{2}{m_V^2}(kE_p - \omega p\cos\theta)^2 + \frac{m_V^2}{2}, \tag{B20}$$

we find

$$\Gamma^{\rm Prod}_{T(L)} = \frac{\alpha}{\omega k}\int_{\frac{\omega}{2}-\frac{k}{2}\sqrt{1-4\frac{m_f^2}{m_V^2}}}^{\frac{\omega}{2}+\frac{k}{2}\sqrt{1-4\frac{m_f^2}{m_V^2}}} dE_p \tag{B21}$$

$$\times F^{T(L)}(\omega, p, \theta)n(E_p)n(\omega - E_p), \tag{B22}$$

where k relates to the dark vector, p/q to the fermions in the loop and $\cos\theta = \frac{\omega E_p}{kp} - \frac{m_V^2}{2pk}$.

APPENDIX C: HADRONIC PRODUCTION

To model hadronic freeze-in production, we treat the coalescence of charged pions into dark photons as a scalar QED process. The spin-summed matrix element is

$$\sum|\mathcal{M}_{s\bar{s}}|^2 = 4\pi\alpha_{\rm eff}^{\pi\pi}m_V^2\left(1 - 4\frac{m_s^2}{m_V^2}\right), \tag{C1}$$

with the massless limit being a factor of 4 smaller than the fermionic case (8). We include the ρ-resonance in the charged-pion interaction via an effective scalar electromagnetic coupling which becomes m_V dependent, $\alpha_{\rm eff}^{\pi\pi}(m_V) = \kappa^2\alpha^{\pi\pi}(\sqrt{s} = m_V)$. The coupling function $\alpha^{\pi\pi}(\sqrt{s})$ is extracted numerically from the $e^+e^- \to \gamma^* \to \pi^+\pi^-(\gamma)$ cross section measured by BaBar Collaboration [51], and similarly for the charged kaons [52].

In accounting for thermal effects, the imaginary part of the polarization tensor can be found in the same manner as in Appendix B, by separating the matrix element into the different propagation modes for scalars,

$$F_s^T = p^2\sin^2\theta, \tag{C2}$$

$$F_s^L = \frac{1}{m_V^2}(kE_p - \omega p\cos\theta)^2, \tag{C3}$$

and (B22) can be used with Bose-Einstein statistics.

The real part of the polarization tensor needs to be derived from first principles in finite-temperature field theory as the ω/k scaling of (B10) (B11) does not generally hold. However, it is known [53] that the high temperature limit is the same as (B2), since the statistics integrals $\int_0^\infty dppn_B(p) = 2\int_0^\infty dppn_F(p)$ compensate for the missing spin degrees of freedom [54]. On account of the high resonant temperature (B6), we find that we can maintain good numerical accuracy with the simple rescaling,

$$\mathrm{Re}^{\rm s}_{\rm T(L)} = \frac{\mathrm{Re}\Pi_{T(L)}}{2}\frac{\int dp\frac{p^2}{E}n_B(E)}{\int dp\frac{p^2}{E}n_F(E)}. \tag{C4}$$

APPENDIX D: BBN ANALYSIS

Here we provide some additional details regarding the treatment of BBN; the analysis of meson injection draws in large part from our previous paper [4] to which we refer the reader for an exhaustive discussion. The Boltzmann code that we use is based on Ref. [55], but incorporates some significant improvements and updates. These are likewise detailed in [4]. Our SBBN yields are in excellent agreement with those presented in [18] at the WMAP value of $\eta_b = 6.2\times10^{-10}$ and with a neutron lifetime of $\tau_n = 885.7$ s.

Below the di-pion threshold, $m_V \leq 2m_{\pi^\pm} = 279$ MeV, only electromagnetic energy injection from V decays is relevant. As discussed in Sec. III, the formation of a photon cascade $f_\gamma(E_\gamma)$ gives way to photodissociation of nuclei. The rate of destruction of a species N with number density n_N is then given by

$$\Gamma_{\rm ph}(T) = 2n_N\int_{E_{\rm thr}}^{E_{\rm max}} dE_\gamma f_\gamma(E_\gamma)\sigma_{\gamma+N\to X}(E_\gamma), \tag{D1}$$

where $\sigma_{\gamma+N\to X}(E_\gamma)$ is the photodissociation cross section for $\gamma + N \to X$ with threshold $E_{\rm thr}$. The factor of two accounts for the back-to-back $e^\pm$ pair forming two independent cascades, each with a maximum energy of $E_{\rm max} = \max\{E_{\rm pair}, E_{\rm inj}/2\}$. We take into account all relevant light element reactions listed in [56] and we also include secondary processes which may result in production of ^{6}Li. The Boltzmann equations describing the temperature evolution of the light elements in the presence of energy injection are straightforward to obtain.

With regard to the injection of mesons and nucleons, we restrict ourselves to reactions at threshold, assuming that charged pions and kaons are thermalized before reacting. Likewise we assume that neutrons will be slowed down by their magnetic moment interaction with electrons, positrons and photons and neglect neutral kaons altogether because of their inability to stop and the associated uncertainty in reaction cross section.

We expect such an approximation to result in more conservative constraints. Incomplete thermalization for charged mesons only happens on the whole for temperatures $T < 40$ keV, for which the plasma stopping power diminishes. Away from threshold, pion-nucleon reactions can proceed resonantly, e.g. $\pi^- p \to \Delta^0 \to \pi^0 n$, with an efficiency up to ~20–30 times the value for stopped pions. Likewise, the total inelastic π^--^{4}He cross section becomes significantly larger for pion kinetic energies of ~150 MeV. Such enhancements as well as nonthermal neutrons with spallating power lead to stronger departures from the standard case and are therefore more strictly constrained. There is, however, the beneficiary effect of reducing the

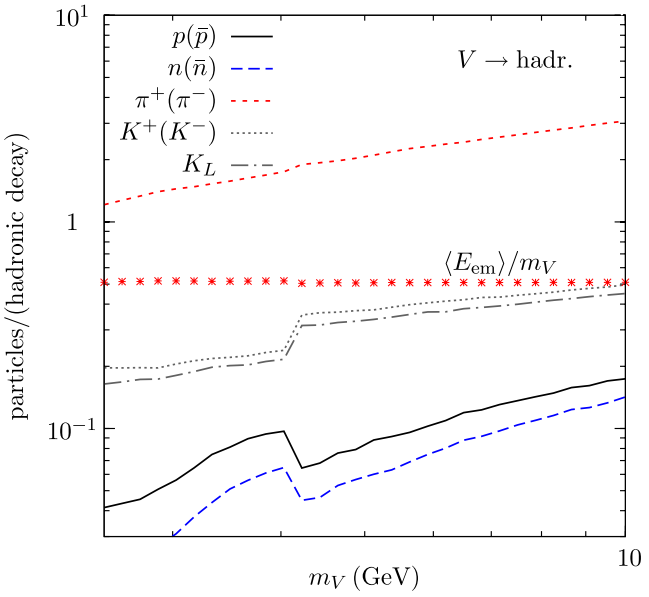

FIG. 10 (color online). The average number of particles per V decay with $m_V > 2.5$ GeV, from a PYTHIA simulation. Also shown is the average electromagnetic energy injected after all particles have decayed to electrons and photons (e^+ are assumed to have annihilated on e^-.) When including leptonic channels, to a good approximation 1/3 of the energy is carried away in the form of neutrinos. Resonances like J/ψ are not captured by the resolution of the simulation and we neglect such isolated points in the parameter space.

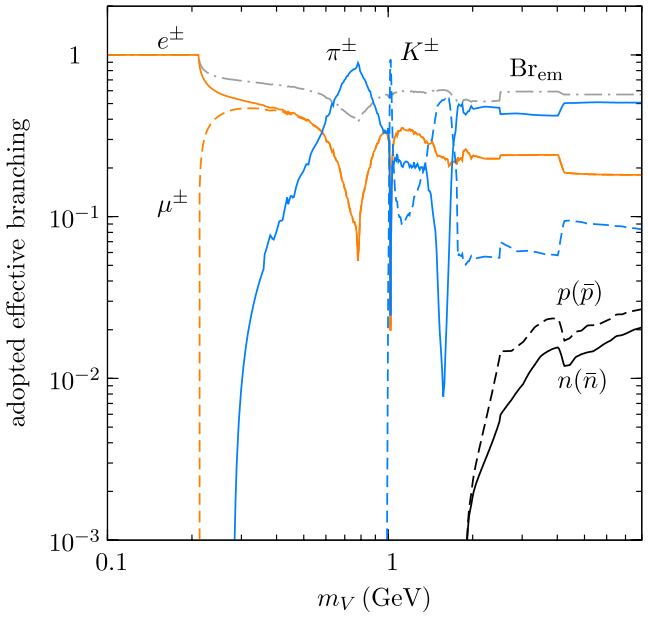

FIG. 11 (color online). The adopted effective branching ratios into the various final states that are relevant for BBN considerations. As multi-pion and kaon states become relevant in the kinematically allowed region, we stitch together BaBar measurements of the $e^\pm \to \pi^\pm$ and $e^\pm \to K^\pm$ cross sections up to $m_V = 1.8$ GeV with our PYTHIA simulation for $m_V \geq 2.5$ GeV. In this plot, any branching to K_L was neglected. Also shown is the fraction of vector mass that is converted into EM-energy, denoted $\mathrm{Br_{em}}$.

cosmological lithium abundance towards observationally favored values through the production of "extra neutrons." As pointed out in [4], this process can also be boosted by the above resonances. However, this solution of the lithium problem is challenged by the simultaneous tightening of the D/H constraint, especially in light of the new D/H determinations discussed in the BBN section. For the interested reader, we point out that a detailed quantitative discussion of incomplete stopping can be found in our preceding work [4].

Finally, baryon/antibaryon pairs can be produced directly in the decay of the vector for $m_V \gtrsim 2$ GeV. Upon injection, resonances and hyperons decay to (anti) protons and (anti)neutrons—possibly accompanied pions and kaons—before interacting with the ambient medium. The fate of the final state nucleons is then as follows: $\bar{n}$ and $\bar{p}$ will preferentially annihilate on protons which are the most abundant target in the Universe with an annihilation cross section $\langle \sigma_{\rm ann} v\rangle \sim m_{\pi^\pm}^{-2}$. Depending on the n/p ratio, they also annihilate with neutrons with a similar cross section. The annihilation on protons is faster than the Hubble rate at all relevant temperatures and—if annihilating on protons—the injection of $n\bar{n}$ results in one net $p \to n$ conversion with associated energy injection of $m_p + m_n$. Likewise, if annihilating on neutrons, $p\bar{p}$ injection results in one net $n \to p$ conversion. Assuming equal cross sections, the relative efficiencies for those processes are $p/(n+p)$ and $n/(n+p)$, respectively, and we treat this sequence of events as being instantaneous.

Neutron injection during BBN in the decay $V \to n\bar{n}$ and close to the threshold $m_V \gtrsim 2m_n$ can be studied by utilizing the (only) measurement of electron-positron annihilation to the neutron-antineutron final state, $e^+e^- \to n\bar{n}$ [57]. At threshold, $\sigma_{e^+e^-\to n\bar{n}} \sim 1$ nb is reported. With a total hadronic cross section $\sigma_{e^+e^-\to \rm had} \sim 50$ nb this points to a branching fraction ~2%. In our actual analysis we use a more conservative value that arises from a joint extraction of the neutron Sachs electric (magnetic) form factor $|G^n_{E(M)}(q^2)|$ in the timelike and spacelike regions; for us, the momentum transfer is timelike with $q^2 = m_V^2$ and

$$\sigma_{e^+e^-\to n\bar{n}} = \frac{4\pi\alpha^2}{3q^2}\sqrt{1-\frac{4m_n^2}{q^2}} \times \left[|G_M^n(q^2)|^2 + \frac{2m_n^2}{q^2}|G_E^n(q^2)|^2\right]. \quad \text{(D2)}$$

At threshold we use the solid black line of Fig. 11 of [58] and the V width is then given by

$$\Gamma_{V\to n\bar{n}} = \kappa^2 \frac{m_V^3}{4\pi\alpha}\sigma_{e^+e^-\to n\bar{n}}(q^2 = m_V^2). \quad \text{(D3)}$$

Away from threshold, we simulate the complex decays of V with PYTHIA. In particular, multipion(kaon) production and decays to hyperons and baryonic resonances become relevant. The yield of phenomenologically relevant final states, $\pi^\pm$, $K^\pm$, K_L, and nucleons is shown in Fig. 10 for $m_V \geq 2.5$ GeV. Narrow resonances like J/ψ are not captured by the resolution of the simulation. The dots in Fig 10 show the average electromagnetic energy injected after all particles have decayed to electrons and photons; e^+ are assumed to have annihilated on e^-. One can see that to a significant fraction of the energy is carried away by neutrinos.

At lower energies, even though the Pythia simulation is not available, the topology of the decay events becomes simpler, and is eventually dominated by two body decays. Above the di-pion (di-kaon) threshold, we therefore use BaBar precision measurements of the $e^\pm \to \pi^\pm$ and $e^\pm \to K^\pm$ cross section until an energy $\sqrt{s} = m_V = 1.8\,\text{GeV}$. Above that energy we stitch the data together with our simulation above, expecting to capture the overall importance of various final states qualitatively correctly. The resulting effective effective branching ratios that are relevant for BBN considerations are shown in Fig. 11. For simplicity, and as alluded to above, we neglect the K_L contribution. Also shown is the fraction of vector mass that is converted into EM-energy in the hadronic decay, denoted by Br_{em}.

[1] R. Essig, J. A. Jaros, W. Wester, P. H. Adrian, S. Andreas, T. Averett, O. Baker, B. Batell *et al.*, arXiv:1311.0029.
[2] B. Holdom, Phys. Lett. **166B**, 196 (1986).
[3] J. Redondo and M. Postma, J. Cosmol. Astropart. Phys. 02 (2009) 005.
[4] M. Pospelov and J. Pradler, Phys. Rev. D **82**, 103514 (2010).
[5] H. An, M. Pospelov, and J. Pradler, Phys. Lett. B **725**, 190 (2013).
[6] H. An, M. Pospelov, and J. Pradler, Phys. Rev. Lett. **111**, 041302 (2013).
[7] J. Redondo and G. Raffelt, J. Cosmol. Astropart. Phys. 08 (2013) 034.
[8] J. D. Bjorken, R. Essig, P. Schuster, and N. Toro, Phys. Rev. D **80**, 075018 (2009); M. Pospelov, Phys. Rev. D **80**, 095002 (2009); H. Davoudiasl, H.-S. Lee, and W. J. Marciano, Phys. Rev. D **86**, 095009 (2012); M. Endo, K. Hamaguchi, and G. Mishima, Phys. Rev. D **86**, 095029 (2012); D. Babusci *et al.* (KLOE-2 Collaboration), Phys. Lett. B **720**, 111 (2013); F. Archilli, D. Babusci, D. Badoni, I. Balwierz, G. Bencivenni, C. Bini, C. Bloise, V. Bocci *et al.*, Phys. Lett. B **706**, 251 (2012); P. Adlarson *et al.* (WASA-at-COSY Collaboration), Phys. Lett. B **726**, 187 (2013); S. Abrahamyan *et al.* (APEX Collaboration), Phys. Rev. Lett. **107**, 191804 (2011); H. Merkel *et al.* (A1 Collaboration), Phys. Rev. Lett. **106**, 251802 (2011); M. Reece and L. -T. Wang, J. High Energy Phys. 07 (2009) 051; J. B. Dent, F. Ferrer, and L. M. Krauss, arXiv:1201.2683; H. K. Dreiner, J.-F. Fortin, C. Hanhart, and L. Ubaldi, Phys. Rev. D **89**, 105015 (2014); S. Andreas, C. Niebuhr, and A. Ringwald, Phys. Rev. D **86**, 095019 (2012); J. Blumlein and J. Brunner, Phys. Lett. B **701**, 155 (2011); R. Essig, R. Harnik, J. Kaplan, and N. Toro, Phys. Rev. D **82**, 113008 (2010); B. Batell, M. Pospelov, and A. Ritz, Phys. Rev. D **80**, 095024 (2009); S. N. Gninenko, Phys. Rev. D **85**, 055027 (2012); Phys. Lett. B **713**, 244 (2012).
[9] J. P. Lees *et al.* (*BaBar* Collaboration), arXiv:1406.2980; D. Babusci *et al.* (KLOE-2 Collaboration), arXiv:1404.7772; H. Merkel, P. Achenbach, C. A. Gayoso, T. Beranek, J. Bericic, J. C. Bernauer, R. Boehm, D. Bosnar *et al.*, arXiv:1404.5502; J. Blumlein and J. Brunner, Phys. Lett. B **731**, 320 (2014).
[10] M. Pettini and R. Cooke, Mon. Not. R. Astron. Soc. **425**, 2477 (2012).
[11] R. Cooke, M. Pettini, R. A. Jorgenson, M. T. Murphy, and C. C. Steidel, arXiv:1308.3240.
[12] S. Burles and D. Tytler, Astrophys. J. **507**, 732 (1998).
[13] D. Kirkman, D. Tytler, N. Suzuki, J. M. O'Meara, and D. Lubin, Astrophys. J. Suppl. Ser. **149**, 1 (2003).
[14] N. Prantzos, E. Vangioni-Flam, and M. Cassé, *Proceedings of Origin and Evolution of the Elements* (Cambridge University Press, Cambridge, England, 1993).
[15] Y. I. Izotov and T. X. Thuan, Astrophys. J. **710**, L67 (2010).
[16] E. Aver, K. A. Olive, R. L. Porter, and E. D. Skillman, J. Cosmol. Astropart. Phys. 11 (2013) 017.
[17] F. Spite and M. Spite, Astron. Astrophys. **115**, 357 (1982).
[18] R. H. Cyburt, B. D. Fields, and K. A. Olive, J. Cosmol. Astropart. Phys. 11 (2008) 012.
[19] B. D. Fields, Annu. Rev. Nucl. Part. Sci. **61**, 47 (2011).
[20] X.-L. Chen and M. Kamionkowski, Phys. Rev. D **70**, 043502 (2004).
[21] L. Zhang, X. Chen, M. Kamionkowski, Z.-g. Si, and Z. Zheng, Phys. Rev. D **76**, 061301 (2007).
[22] D. Blas, J. Lesgourgues, and T. Tram, J. Cosmol. Astropart. Phys. 07 (2011) 034.
[23] B. Audren, J. Lesgourgues, K. Benabed, and S. Prunet, J. Cosmol. Astropart. Phys. 02 (2013) 001.
[24] P. A. R. Ade *et al.* (Planck Collaboration), arXiv:1303.5075.
[25] C. L. Bennett *et al.* (WMAP Collaboration), Astrophys. J. Suppl. Ser. **208**, 20 (2013).
[26] E. Komatsu *et al.* (WMAP Collaboration), Astrophys. J. Suppl. Ser. **192**, 18 (2011).
[27] R. Keisler, C. L. Reichardt, K. A. Aird, B. A. Benson, L. E. Bleem, J. E. Carlstrom, C. L. Chang, H. M. Cho *et al.*, Astrophys. J. **743**, 28 (2011).

[28] T. R. Slatyer, N. Padmanabhan, and D. P. Finkbeiner, Phys. Rev. D **80**, 043526 (2009).
[29] N. Padmanabhan and D. P. Finkbeiner, Phys. Rev. D **72**, 023508 (2005).
[30] T. R. Slatyer, Phys. Rev. D **87**, 123513 (2013).
[31] J. M. Cline and P. Scott, J. Cosmol. Astropart. Phys. 03 (2013) 044; 05 (2013) E01.
[32] B. Batell, M. Pospelov, and A. Ritz, Phys. Rev. D **79**, 115008 (2009).
[33] M. Pospelov, A. Ritz, and M. B. Voloshin, Phys. Rev. D **78**, 115012 (2008).
[34] E. Aprile, K. Arisaka, F. Arneodo, A. Askin, L. Baudis, A. Behrens, K. Bokeloh, E. Brown *et al.*, Phys. Rev. D **83**, 082001 (2011); **85**, 029904(E) (2012).
[35] K. Arisaka, P. Beltrame, C. Ghag, J. Kaidi, K. Lung, A. Lyashenko, R. D. Peccei, P. Smith, and K. Ye, Astropart. Phys. **44**, 59 (2013).
[36] K. Abe *et al.* (XMASS Collaboration), arXiv:1406.0502.
[37] A. Ibarra, D. Tran, and C. Weniger, Int. J. Mod. Phys. A **28**, 1330040 (2013).
[38] O. Adriani *et al.* (PAMELA Collaboration), Nature (London) **458**, 607 (2009).
[39] M. Aguilar *et al.* (AMS Collaboration), Phys. Rev. Lett. **110**, 141102 (2013).
[40] A. Esmaili, A. Ibarra, and O. L. G. Peres, J. Cosmol. Astropart. Phys. 11 (2012) 034.
[41] K. Murase and J. F. Beacom, J. Cosmol. Astropart. Phys. 10 (2012) 043.
[42] D. Walker *et al.* (to be published); A. Fradette *et al.* (to be published).
[43] M. Hindmarsh and O. Philipsen, Phys. Rev. D **71**, 087302 (2005).
[44] S. Borsanyi, Z. Fodor, C. Hoelbling, S. D. Katz, S. Krieg, and K. K. Szabo, Phys. Lett. B **730**, 99 (2014).
[45] N. Haque, A. Bandyopadhyay, J. O. Andersen, M. G. Mustafa, M. Strickland, and N. Su, J. High Energy Phys. 05 (2014) 027.
[46] S. Borsanyi, G. Endrodi, Z. Fodor, A. Jakovac, S. D. Katz, S. Krieg, C. Ratti, and K. K. Szabo, J. High Energy Phys. 11 (2010) 077.
[47] Y. Aoki, G. Endrodi, Z. Fodor, S. D. Katz, and K. K. Szabo, Nature (London) **443**, 675 (2006).
[48] S. Borsanyi, Z. Fodor, C. Hoelbling, S. D. Katz, S. Krieg, C. Ratti, and K. K. Szabó, J. High Energy Phys. 09 (2010) 073.
[49] E. Braaten and D. Segel, Phys. Rev. D **48**, 1478 (1993).
[50] H. A. Weldon, Phys. Rev. D **28**, 2007 (1983).
[51] J. P. Lees *et al.* (*BaBar* Collaboration), at BABAR," Phys. Rev. D **86**, 032013 (2012).
[52] J. P. Lees *et al.* (*BaBar* Collaboration), Phys. Rev. D **88**, 032013 (2013).
[53] J. I. Kapusta and C. Gale, *Finite-temperature Field Theory: Principles and Applications* (Cambridge University Press, Cambridge, England, 2006).
[54] V. S. Rychkov and A. Strumia, Phys. Rev. D **75**, 075011 (2007).
[55] L. Kawano, Report No. FERMILAB-PUB-92-004-A.
[56] R. H. Cyburt, J. R. Ellis, B. D. Fields, and K. A. Olive, Phys. Rev. D **67**, 103521 (2003).
[57] A. Antonelli, R. Baldini, P. Benasi, M. Bertani, M. E. Biagini, V. Bidoli, C. Bini, T. Bressani *et al.*, Nucl. Phys. **B517**, 3 (1998).
[58] E. L. Lomon and S. Pacetti, Phys. Rev. D **85**, 113004 (2012); **86**, 039901(E) (2012).